CRYSTAL GROWTH & DESIGN

Article

Cite This: Cryst. Growth Des. 2018, 18, 4952−4962

pubs.acs.org/crystal

Effect of Temperature Cycling on Ostwald Ripening

Thijs van Westen*,† and Robert D. Groot*,‡

†Institute AMOLF, Science Park 104, 1098XG, Amsterdam, The Netherlands

‡Unilever Research & Development, Olivier van Noortlaan 120, 3133AT Vlaardingen, The Netherlands

ABSTRACT: We study the effect of temperature cycling on the rate of Ostwald ripening (or coarsening) of spherical particles dispersed in a binary solution. A widespread view, which states a temperature cycle generally enhances the rate of Ostwald ripening by first dissolving the smallest particles (heating) and then regrowing the dissolved amount of material on the remaining particles (cooling), is shown to be inadequate as it does not include transient effects. On the basis of a simulation method that assumes mass transfer as the limiting growth mechanism, we show that each temperature cycle is followed by a significant relaxation of the particle-size distribution, during which the number of particles remains constant, and the average particle size *decreases*. The relaxation is shown to be crucial to obtain a linear scaling of the average particle radius cubed with the number of cycles applied (or time), which is the behavior generally observed for the evolution of ice crystals in cycling experiments on frozen aqueous solutions or frozen foods. We show the experimentally observed increase in the proportionality constant (or "coarsening rate") as compared to isothermal ripening, or the increase of the coarsening rate with increasing cycle frequency, can be reproduced convincingly only if some (transient) ripening is allowed to take place at the elevated temperature of each cycle. Our results thus suggest the effect of temperature cycling on Ostwald ripening is governed by a dissolution−ripening−regrowth−relaxation mechanism.

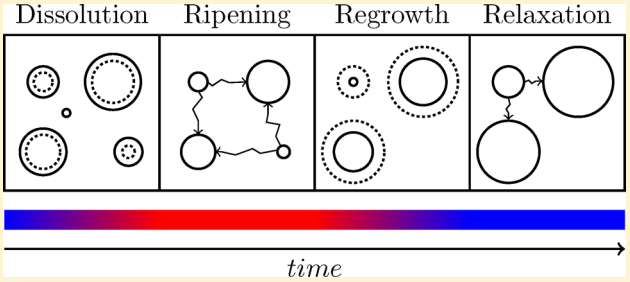

1. INTRODUCTION

Many systems relevant to practical applications (e.g., food emulsions, metallic alloys, pharmaceuticals, and heterogeneous catalysts) comprise a mixture of second-phase particles (or droplets) dispersed within a bulk matrix. Typically these systems are at the latest stage of a first-order phase transition, where the global supersaturation approaches zero, and the primary driving force to restore equilibrium reduces to a minimization of the surface area (more specifically the free energy associated with it) between phases. This process, generally referred to as Ostwald ripening, or coarsening,[1−3] typically increases the size scale of the second phase (e.g., the average particle size), leading to a coarser microstructure, and, in many cases, a loss in product quality. To gain better control over such quality losses requires a fundamental understanding of the physical mechanisms at play.

For isothermal conditions, Ostwald ripening has been widely studied, and the underyling physical mechanisms are relatively well understood. Much of the understanding dates back to 1961, when Lifshitz, Slyozov, and Wagner (LSW)[4,5] developed a theory for describing the late-stage dynamics of first-order phase transitions. For both, bulk mass-transfer and attachment-kinetics as the limiting growth mechanism, LSW predicted the existence of a stationary regime, during which the distribution of particle sizes evolves self-similarly upon rescaling with some characteristic length scale (e.g., the average particle size). The characteristic length scale raised to a certain power (the value of which depending on the rate-limiting growth mechanism) was shown to scale linearly with time, the proportionality constant, or "coarsening rate", thereby fully determining the growth dynamics. Both, the scaling characteristics of the characteristic length scale, and the self-similarity of the rescaled particle-size distribution (PSD), have been confirmed qualitatively by experiments (mostly in metallurgy, see, e.g., Ratke and Voorhees[3] or Mullins[6] and references therein). The search for quantitative agreement between theory and experiments remains an active area of research, however, facing many difficulties in material property estimation or in limitations inherent to the LSW approach itself.[7−11] Several extensions of the LSW theory have been developed; examples include treatment of the effects of dispersed-phase volume fraction,[12−18] different growth mechanisms (joining of two particles), (Brownian) particle movement, and spatial correlations between particles. For a review, see Ratke and Voorhees.[3]

It has long been recognized that cyclic fluctuations in temperature (from a low temperature to an elevated temperature and back) provide an additional mechanism for coarsening. Experimental examples include the enhanced coarsening of ice crystals in (model systems of) frozen foods or biomaterials due to freeze−thaw cycling,[19−22] the enhanced coarsening of crystals in igneous rock under thermal cycling induced by volcanic activity,[23−25] and temperature treatment (annealing) of metals. The explanation generally put forward is

Received: February 19, 2018
Revised: May 17, 2018
Published: July 16, 2018

DOI: 10.1021/acs.cgd.8b00267
Cryst. Growth Des. 2018, 18, 4952−4962

a dissolution−regrowth mechanism:[23,25−28] first, the smallest particles in the system dissolve upon heating, leading to a system of fewer nuclei. Second, upon cooling, the dissolved amount of material is regrown on the remaining nuclei, leading to larger particles. In the present work, we show this picture does indeed capture an important part of the physics required to describe cycling-enhanced Ostwald ripening. It is not complete, however.

By combining (1) the analytical theory of stationary (isothermal) Ostwald ripening, (2) a scaling Ansatz for diffusion-limited growth during heating and cooling, and (3) a numerical calculation method for transient (nonstationary) ripening, we show each temperature cycle is followed by some *relaxation* of the particle-size distribution, which significantly affects the temporal evolution of the average particle size. Our numerical results indicate that the average particle size decreases during relaxation, and that if relaxation is allowed to complete, the decrease is always stronger than the increase induced by dissolution−regrowth. Our results thus show that, for a single temperature cycle plus relaxation to lead to enhanced particle growth as compared to isothermal Ostwald ripening, some ripening (which is transient) needs to take place at the peak temperature of the cycle.

For successive cycling, we show the relaxation in between cycles ultimately causes a linear scaling of the average particle radius cubed with the number of applied cycles (or time), which is the same scaling as predicted for isothermal Ostwald ripening, confirming the results of several experimental cycling studies.[19,22,29−31] If initially the cycle time is longer than the time needed for the PSD to relax back to its stationary form, we find two linear regimes, the crossover between them being determined by the cycle number where the relaxation time (which grows with each cycle) starts to exceed the cycle time (which is kept constant). If no Ostwald ripening is allowed to take place at the elevated temperature of a cycle, the first regime is characterized by a coarsening rate that is slightly smaller than for isothermal ripening, which is in contrast to what is observed experimentally.[19−22,24,25] If ripening at the elevated temperature is allowed, both regimes are characterized by faster Ostwald ripening as compared to the isothermal case, which is in line with experimental results.

We conclude the correct mechanism for cycling-enhanced Ostwald ripening is dissolution−ripening−regrowth−relaxation. We consider this as the main insight of this work.

2. SYSTEM DEFINITION

We consider a system of volume V and temperature T_L, comprising a two-phase mixture of N spherical particles (β-phase) of species 1, dispersed within a binary matrix (α-phase) of species 1 and 2. The particles are assumed fixed in space and of uniform density. The interface between particles and matrix is assumed sharp, inducing a stepwise change in composition and densities between phases.

At any instant in time t, the distribution of particle radii $\boldsymbol{a} = (a_1, a_2,\cdots,a_N)_t$ is described by a single-particle density $n(\mathbf{r},a,t)$, which, under multiplication with $\mathrm{d}a\ \mathrm{d}\mathbf{r}$, describes the number of particles of size between a and $a + \mathrm{d}a$ in a volume element between $\mathbf{r}$ and $\mathbf{r} + \mathrm{d}\mathbf{r}$. We assume the particles are distributed uniformly throughout the system, allowing the particle density to be written as $n(a,t)$, which can be factorized further as $n(a,t) = n(t)f(a,t)$ where $n(t) = N(t)/V$ is a uniform number density and $f(a,t)$ a particle-size distribution (PSD), which normalizes to unity.

3. ISOTHERMAL OSTWALD RIPENING

Before addressing the issue of temperature variations, we briefly review the basic concepts needed to understand the process of isothermal Ostwald ripening. We limit ourselves to the idealized case of curvature-driven, bulk mass-transfer limited coarsening of spherical particles with isotropic surface energy. Any effects of viscoelastic stress in the surrounding matrix are assumed negligible. For a more complete discussion, the reader is referred to our previous work,[11] Ratke and Voorhees,[3] or to the review article by Voorhees.[32]

At the basis of any theory for Ostwald ripening is a balance equation that describes the rate of change of the particle density $n(a,t)$. In the absence of particle nucleation and accretion/coalescence, the balance equation takes on the form of a continuity equation, according to

$$\frac{\partial n(a,t)}{\partial t} + \frac{\partial}{\partial a} n(a,t)\langle \dot{a} \rangle_a = 0 \tag{1}$$

where $\dot{a} \equiv \mathrm{d}a/\mathrm{d}t$ is the microscopic growth rate of a single particle, and $\langle \cdot \rangle_a$ denotes an average over all particles of size a.

A general equation for the microscopic growth rate $\dot{a}$ can be derived from the species mass balances over the moving interface. In the absence of chemical reactions, it is also allowed to consider molar balances; for the case of a spherical particle of total molar density c^β growing within a matrix of total molar density c^α, one obtains[11]

$$\dot{a} = \left. \frac{-J_{r,i}^{\alpha}(r)}{c^{\beta}(x_i^{\beta} - x_i^{\alpha}(r))} \right|_{r=a} \tag{2}$$

where $J_{r,i}^{\alpha}$ is the radial component of the molar diffusional flux of species i in the matrix (considered positive when directed along the radial coordinate r starting from the center of mass of the particle), and x_i^{α} and x_i^{β} are the molar fractions of species i in the matrix and dispersed phase. As the particle-phase is assumed uniform, only the quantities with superscript "α" are local and need to be evaluated at the surface ($r = a$).

The mole fractions at the particle surface are assumed to satisfy local thermodynamic equilibrium. Due to the effect of curvature on the chemical potential of the species within the particles, the equilibrium compositions are shifted relative to their values at bulk phase equilibrium x_{eq}. For particles of micron-scale or larger, the shift can to a good approximation be obtained from the first-order Gibbs−Thomson equation, which for spherical particles can be written as[11]

$$x_i^{\alpha}(r)|_{r=a} = x_{i,\mathrm{eq}}^{\alpha}\left(1 + \frac{2l_{c,i}}{a}\right) \tag{3}$$

where $l_{c,i}$ is a material-dependent parameter, denoted as the "capillary length", which is calculated as

$$l_{c,i} = \frac{\sigma v_{\mathrm{eq}}^{\beta}(1 - x_{i,\mathrm{eq}}^{\alpha})}{RT\Gamma_{\mathrm{eq}}\Delta x_{i,\mathrm{eq}}} \tag{4}$$

where σ is the surface energy between phases α and β, v^β is the molar volume of the dispersed phase, $\Delta x_{i,\mathrm{eq}} = x_{i,\mathrm{eq}}^{\beta} - x_{i,\mathrm{eq}}^{\alpha}$ is the composition difference at bulk phase equilibrium (i.e., the miscibility gap), R is the gas constant, T is absolute temperature, and $\Gamma = x_i^{\alpha}(\partial\mu_i^{\alpha}/\partial x_i^{\alpha})_{p,T}/RT$ is the thermodynamic factor of the matrix phase, with μ_i^{α} the chemical potential of species i.

DOI: 10.1021/acs.cgd.8b00267
Cryst. Growth Des. 2018, 18, 4952−4962

The diffusional flux from the particle surface into the matrix is obtained from Fick's law, which we define with respect to a molar-averaged reference frame as[33,34]

$$J^{\alpha}_{r,i}(a) = -c^{\alpha}D^{\alpha}\left.\frac{\partial x_i^{\alpha}(r)}{\partial r}\right|_{r=a} \tag{5}$$

with D^{α} the binary Fick diffusion coefficient.

The diffusional flux is affected by curvature through the Gibbs−Thomson condition eq 3, which constitutes the boundary condition for the composition profile at the particle surface. Typically, the effect of curvature on the mole fractions at the surface is negligible *compared to their difference*, that is, $(x_i^{\beta} - x_i^{\alpha}(r))|_{r=a} \approx x^{\beta}_{i,\mathrm{eq}} - x^{\alpha}_{i,\mathrm{eq}} \equiv \Delta x_{i,\mathrm{eq}}$. The microscopic growth rate eq 2 thus simplifies as

$$\dot{a} = \left.\frac{c^{\alpha}D^{\alpha}}{c^{\beta}\Delta x_{i,\mathrm{eq}}}\frac{\partial x_i^{\alpha}(r)}{\partial r}\right|_{r=a} \tag{6}$$

The second boundary condition, namely, the composition at some position in the matrix, is more difficult to define, as it reflects the local environment of a particle, which is generally not known. In the majority of theoretical work on Ostwald ripening, the local environment is treated approximately, based on a statistically averaged composition profile for all particles within a size class a. The averaging generally introduces a dependence of the averaged growth rate $\langle \dot{a} \rangle_a$ on the volume fraction of dispersed-phase material ϕ_{V}, which acts as a global measure for the local environment. We refer to the Supporting Information of a previous work[11] for details on this. Here, we simply use the classical model of LSW,[4] which assumes each particle grows within an infinite medium and thus does not incorporate any volume-fraction effect, and the model of Brailsford and Wynblatt[13] (BW), which was shown to account reasonably well for the effect of nonzero volume fraction on Ostwald ripening.[11] The averaged volumetric growth rate $B(a,\phi_{\mathrm{V}}) \equiv a^2\langle \dot{a} \rangle_a$ obtained from these models can be reformulated to a convenient form, where the dependence on particle size can be reformulated in terms of a scaled variable $z = a/a^*(t)$, with $a^*(t)$ a critical radius that defines the size class with an averaged growth rate of zero (effectively this is a measure for the supersaturation). The result for the LSW theory is

$$B^{\mathrm{LSW}}(z) = 6\xi(z - 1) \tag{7}$$

with ξ is a dimensional prefactor, defined as

$$\xi = \left.\frac{c^{\alpha}l_{c,i}D^{\alpha}x^{\alpha}_{i,\mathrm{eq}}}{c^{\beta}\Delta x_{i,\mathrm{eq}}}\right|_{r=a} \tag{8}$$

The growth rate for the BW model can be written as an extension of the LSW result, according to

$$B^{\mathrm{BW}}(z) = (1 + z/z_s)B^{\mathrm{LSW}}(z) \tag{9}$$

where

$$z_s = \frac{2\langle z^3 \rangle}{3\phi_{\mathrm{V}}\langle z^2 \rangle + \sqrt{9(\phi_{\mathrm{V}}\langle z^2 \rangle)^2 + 12\phi_{\mathrm{V}}\langle z^3 \rangle\langle z \rangle}} \tag{10}$$

is a dimensionless screening length, that effectively takes into account the local environment of particles through a dependence on the volume fraction ϕ_{V}, and several averages $\langle \cdot \rangle$ over the ensemble of particles.

On the basis of the averaged growth rate eq 7 combined with a mass balance constraint for the precipitating species, LSW showed that, asymptotically (i.e., in the limit of long coarsening times), the critical particle radius cubed must scale linearly with time, as

$$a^{*3} = a_0^{*3} + K^*t \tag{11}$$

with the proportionality constant $K^* \equiv \mathrm{d}a^{*3}/\mathrm{d}t$ (called the coarsening rate) calculated as

$$K^* = \frac{8}{9}\xi \tag{12}$$

Additionally, the continuity equation eq 1, growth rate eq 7, and mass balance constraint were shown to constitute a nonlinear integro-differential equation that leads to a unique (stable) asymptotic solution $n(z,t) = f_{\mathrm{eq}}(z)n(t)$. The stationary, self-similar form of the PSD $f_{\mathrm{eq}}(z)$ could be calculated analytically, as

$$f_{\mathrm{eq}}(z) = \frac{4}{9}z^2\left(\frac{3}{3+z}\right)^{7/3}\left(\frac{3/2}{3/2-z}\right)^{11/3}\exp\left(\frac{z}{z-3/2}\right) \tag{13}$$

As the growth rate of the BW model eqs 9−10 contains an implicit dependence on the PSD (through the averages), the stationary PSD and coarsening rate can only be calculated numerically for this model. To not overcomplicate the analysis, we refer to the Supporting Information of our previous work for the respective equations.[11]

Finally, we note that for comparing to experimental data it is generally more useful to consider the coarsening rate for the average particle size, $K = \mathrm{d}\langle a \rangle^3/\mathrm{d}t$. The latter can be related to the coarsening rate of the critical particle size, according to

$$K = K^*\langle z \rangle^3 \tag{14}$$

For the LSW theory, this leads to the simple result $K = K^*$.

4. TEMPERATURE VARIATIONS

4.1. Dimensionless Variables. In the remainder, length and time are made dimensionless using

$$L = a_0^* \tag{15}$$

$$\tau = \left.\frac{a_0^{*3}c^{\beta}\Delta x_{i,\mathrm{eq}}}{c^{\alpha}(a)l_{c,i}D^{\alpha}x^{\alpha}_{i,\mathrm{eq}}}\right|_{T_{\mathrm{L}}} = \frac{a_0^{*3}}{\xi(T_{\mathrm{L}})} \tag{16}$$

with a_0^* the critical radius at the start of the first temperature cycle, and ξ (T_{L}) the dimensional prefactor of eq 7. Dimensionless variables are denoted using a tilde, e.g., dimensionless radius is $\tilde{a}$.

4.2. Model. Initially, the system is assumed self-similar, at a temperature T_{L}. The distribution of particle sizes $(\tilde{a}_1, \tilde{a}_2, \cdots, \tilde{a}_N)_{t_0}$ is generated according to one of the models for isothermal Ostwald ripening as presented in Section 3, using an acceptance-rejection method. Typically, the number of particles is chosen in the range from $N = 5 \times 10^5$ to $N = 10^6$.

At a time t_0, a fluctuation in temperature takes place, a schematic of which is drawn in Figure 1. The fluctuation brings the system to an elevated temperature T_{H} at time t_1, keeps it

DOI: 10.1021/acs.cgd.8b00267
Cryst. Growth Des. 2018, 18, 4952−4962

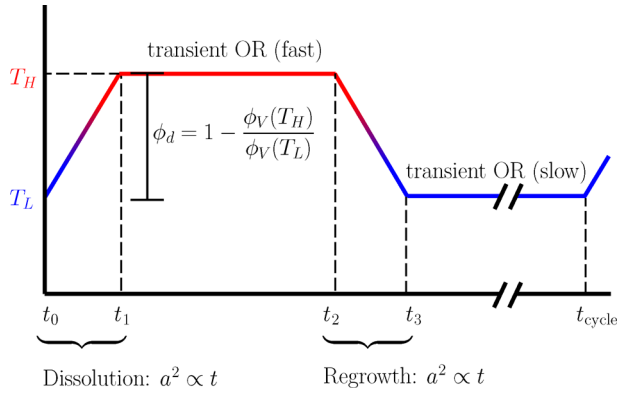

Figure 1. Model used to describe a cycle between a low temperature T_L and high temperature T_H. During temperature variations, growth is assumed to be driven by supersaturation, and governed by the scaling $da^2 \propto dt$. At times t_1 and t_3, the supersaturation is assumed to have decreased sufficiently for (transient) Ostwald ripening (OR) to become the dominant growth mechanism. During these stages, the rescaled PSD slowly "relaxes" back to its stationary form. The amplitude of a cycle is measured by the fraction of material that dissolves upon heating ϕ_d. The time during heating and cooling is assumed negligible compared to the cycle time t_{cycle}. Two different cases are considered, Case 1: no ripening at $T_H(t_2 - t_1 = 0)$, Case 2: ripening at $T_H(t_2 - t_1 > 0)$.

there until time t_2, and brings the system back to T_L at time t_3. At the cycle time t_{cycle} this process is repeated.

The time during heating and cooling is assumed negligible compared to the cycle time, and temperature equilibration is assumed instant. The amplitude of a cycle can hence be defined by the fraction of dispersed-phase material that dissolves upon heating

$$\phi_d = 1 - \frac{\phi_V(T_H)}{\phi_V(T_L)} \tag{17}$$

with $\phi_V(T)$ the *equilibrium* volume fraction of dispersed phase. Note we herewith neglected any small changes in system volume with temperature.

The growth during heating (dissolution, $t_0 \rightarrow t_1$) and cooling (regrowth, $t_2 \rightarrow t_3$) is assumed fast and driven solely by supersaturation. As an approximate growth law, the change in surface of the particles is assumed to scale linearly with time

$$|da^2| \propto dt \tag{18}$$

which is the behavior generally found in numerical simulation studies on bulk-mass-transfer-limited growth of spherical particles under large supersaturation.[35,36] Any changes in shape of the particles due to large gradients in supersaturation (e.g., dendritic growth)[37−39] or due to a roughening transition are neglected. For any particle of index i, it follows that

$$\tilde{a}_i^2(t_1) = \tilde{a}_i^2(t_0) - \lambda \tag{19}$$

$$\tilde{a}_i^2(t_3) = \tilde{a}_i^2(t_2) + \lambda' \tag{20}$$

with constants λ and λ' fixed by the assumption of thermal equilibration, as

$$1 - \phi_d = \frac{\sum_{i=1}^N \tilde{a}_i^3(t_1)}{\sum_{i=1}^N \tilde{a}_i^3(t_0)}$$

$$\frac{1}{1 - \phi_d} = \frac{\sum_{i=1}^N \tilde{a}_i^3(t_3)}{\sum_{i=1}^N \tilde{a}_i^3(t_2)} \tag{21}$$

These equations must be solved iteratively.

During $t_1 \rightarrow t_2$ and $t_3 \rightarrow t_{cycle}$, the supersaturation is assumed to have dropped sufficiently for curvature effects to become important and for growth to proceed by the mechanism of (transient) Ostwald ripening. During these stages the perturbed PSD (partly) relaxes back toward its stationary form, under the action of one the volumetric growth rates $B_i(\tilde{a}_i/\tilde{a}^*, \phi_V(T))$ of Section 3.

The required critical radius $\tilde{a}^*$ is calculated based on the assumption of constant phase volumes (see ref 40 for some discussion on this), according to

$$\sum_{i=1}^N B_i(\tilde{a}_i/\tilde{a}^*, \phi_V(T)) = 0 \tag{22}$$

For both growth models analyzed in this paper, this can be solved analytically, as

$$\tilde{a}^* = \begin{cases} \langle \tilde{a} \rangle & \text{(LSW)} \\ \langle \tilde{a} \rangle \left(1 + \frac{1}{z_s} \left[\frac{\langle z^2 \rangle}{\langle z \rangle} - 1 \right] \right) & \text{(BW)} \end{cases} \tag{23}$$

with the screening length z_s defined by eq 10.

Once the critical particle radius is calculated, the dimensionless growth rate $\tilde{B}_i$ can be evaluated for all particles in the system, after which their size is updated over a time-step $\Delta\tilde{t}$, according to

$$\tilde{a}_{i,new}^3 = \tilde{a}_i^3 + \psi \tilde{B}_i(\tilde{a}_i/\tilde{a}^*, \phi_V(T))\Delta\tilde{t} \tag{24}$$

with a default value of $\Delta\tilde{t} = 0.001$. If particles dissolve completely within a time frame smaller than this value, the size of the time-step is adjusted so that only one particle dissolves. If one does not follow this procedure, but let multiple particles dissolve within one time step, eq 22 is violated.

The scale-factor ψ accounts for the fact that ripening at the elevated temperature T_H proceeds at a faster rate than at the low temperature T_L. It is defined as

$$\psi = \begin{cases} \frac{\tau|_{T_L}}{\tau|_{T_H}} = \frac{\xi(T_H)}{\xi(T_L)} & \text{if } t_1 < t < t_2 \\ 1 & t_3 < t < t_{cycle} \end{cases} \tag{25}$$

with ξ the dimensional prefactor of eq 8. For the time being, one can consider ψ as an additional model parameter for the case that $t_2 - t_1 > 0$.

During the simulations, we sample the number of particles in the system N, the average particle size $\langle \tilde{a} \rangle$, the critical radius $\tilde{a}^*$, the rescaled PSD $f(z,\tilde{t})$, and two measures for the effect of a temperature cycle, namely the fraction of particles that survives

$$\chi(t) = \frac{N(t)}{N(t_0)} \tag{26}$$

and the growth factor

DOI: 10.1021/acs.cgd.8b00267
Cryst. Growth Des. 2018, 18, 4952−4962

$$G(t) = \frac{\langle a\rangle^3(t)}{\langle a\rangle^3(t_0)} \tag{27}$$

If successive cycles are applied, these metrics are given an index n for indicating the cycle number; t_0 then applies to the starting time of the respective cycle.

5. RESULTS AND DISCUSSION

We analyze two different scenarios, which can be considered as limiting cases. The first scenario, denoted as Case 1, assumes there to be no Ostwald ripening at the elevated temperature at all, implying $t_2 - t_1 = 0$. The second scenario, denoted as Case 2, defines the situation for which some ripening occurs at the elevated temperature, implying $t_2 - t_1 > 0$.

5.1. Case 1: $t_2 - t_1 = 0$. Figure 2 shows the time evolution of the rescaled PSD, the number of particles N, and the average particle radius cubed $\langle\tilde{a}\rangle^3$, after applying a temperature cycle of amplitude $\phi_d = 0.9$ to a stationary LSW distribution.

The temperature cycle significantly alters the shape of the PSD, the most prominent effect being a cutoff of the lower tail. Only a fraction $\chi(t_3) \approx 0.57$ of the particles survives, leading to a increase in the average particle size by a growth factor $G(t_3) \approx 2$ after dissolution-regrowth.

The relaxation toward the stationary regime is characterized by two stages. In the first stage, the tail of the PSD has not fully grown back to $z = 0$, and, accordingly, the number of particles remains constant. Since the process we are simulating is in fact an exchange in phase volume from small to large particles, the radii of the small particles in the system decrease by a larger factor than the radii of the large particles increase. As the number of particles remains constant during this stage, the average particle radius must thus decrease. This is exactly what is observed in Figure 2C. As time proceeds, the small particles grow smaller, leading to an enhancement of this effect. The result is an increasingly negative slope $\mathrm{d}\langle\tilde{a}\rangle^3/\mathrm{d}\tilde{t}$ with $\tilde{t}$ in Figure 2C. As soon as the tail of the PSD has grown back to $z = 0$, the smallest particles start to dissolve, and the normal process of Ostwald ripening (i.e., a decreasing number of particles and increasing average particle size) sets in. This part is denoted as the second stage. As can be observed, the relaxation of the PSD almost exclusively takes place during the first stage. We therefore define a relaxation time t_{relax}, as the time where stage 1 changes to stage 2. Eventually, the stationary LSW distribution and the stationary value of the coarsening rate $\tilde{K} = 8/9$ are recovered.

As we show in Figure 2C, the decrease in average particle size during relaxation is stronger than the growth induced by the temperature cycle (via dissolution−regrowth), leading to a net decrease of the average particle size compared to isothermal Ostwald ripening, i.e.,

$$G(t_{relax}) < 1 + \tilde{K}^*(T_L)\tilde{t}_{relax} \tag{28}$$

We find that this somewhat surprising result is unaffected by the choice of growth model, or the magnitude of a temperature cycle (Figure 3). If the traditional dissolution−regrowth model of a temperature cycle is extended by a description of relaxation effects taking place after regrowth, the net effect of a single temperature cycle is thus a retardation of growth compared to isothermal ripening.

For successive cycling, we find the behavior is slightly more complicated. As shown in Figure 4, two different regimes can be observed, depending on the relative magnitude of the relaxation time (which grows with each cycle) and the cycle time (which is constant). If the relaxation time is smaller than the cycle time, the PSD fully relaxes in between cycles. The behavior due to successive cycling is then the same as observed

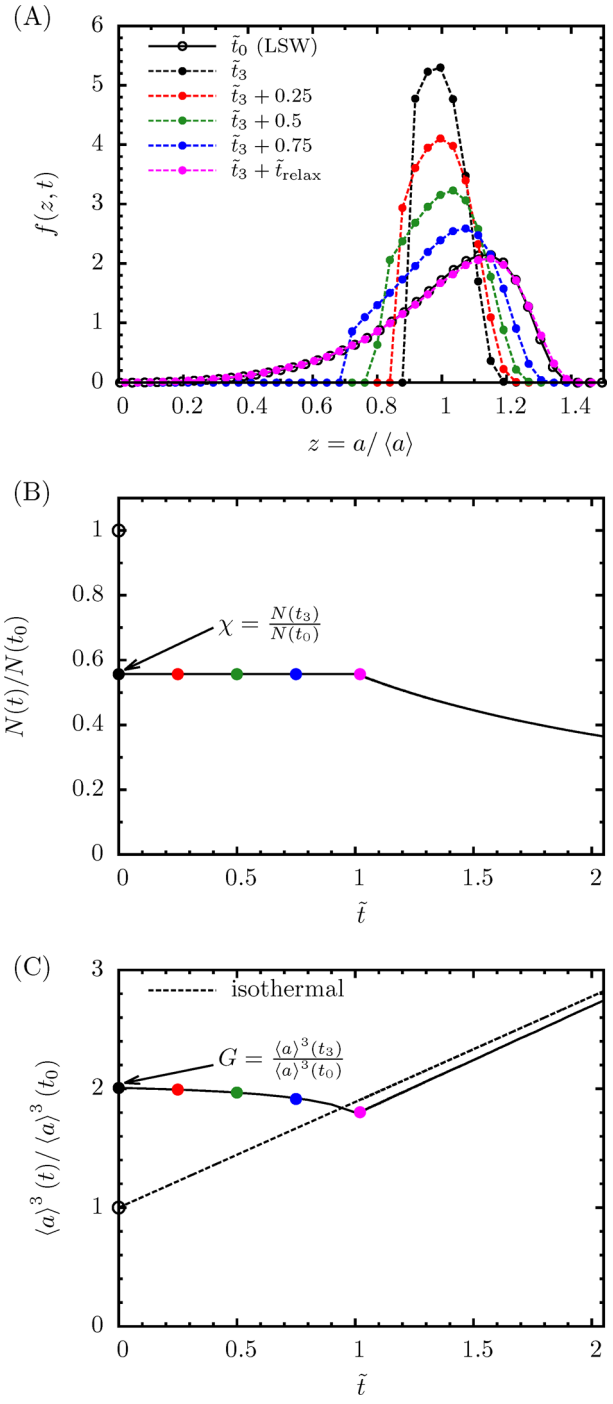

Figure 2. Temporal evolution of the rescaled PSD $f(z)$ (A), the number of particles N (B), and the average particle radius cubed $\langle a\rangle^3$ (C), after applying a temperature cycle of amplitude $\phi_d = 0.9$ and $\tilde{t}_2 - \tilde{t}_1 = 0$ at $\tilde{t} = 0$ (see Figure 1 for schematic). Results were obtained using the growth rate of LSW. Both, the stationary form of the LSW distribution and the correct coarsening rate are retained after sufficiently long simulation time. The relaxation time $\tilde{t}_{relax}$ is defined as the time needed for the PSD to just have grown back to $z = 0$. In (B), this is the point where the number of particles starts to decrease. As can be observed in (A), the relaxation at that point is very close to complete. For the case analyzed in this figure, $\tilde{t}_{relax} \approx \tilde{t}_3 + 1.19$.

DOI: 10.1021/acs.cgd.8b00267
Cryst. Growth Des. 2018, 18, 4952−4962

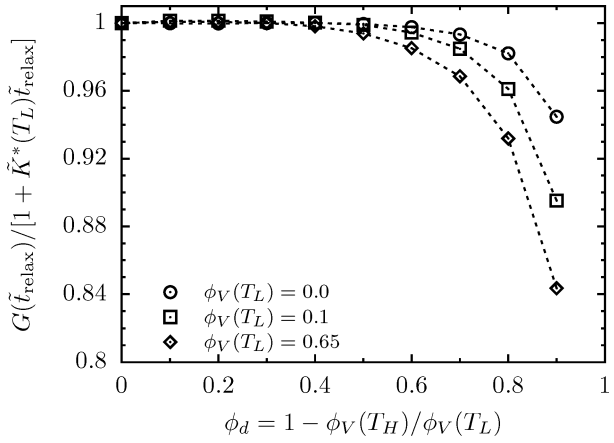

Figure 3. Growth factor after a temperature cycle with full relaxation $G(t_{relax})$ (for details see Figure 2) relative to the growth factor for a same amount of time during isothermal Ostwald ripening at T_L. The effect of volume-fraction was calculated using the BW theory. Lines are a guide for the eye. The main insight obtained from this figure is that for Case 1 of a temperature cycle ($t_2 - t_1 = 0$), the net effect of a temperature cycle plus relaxation is slower growth as compared to isothermal ripening.

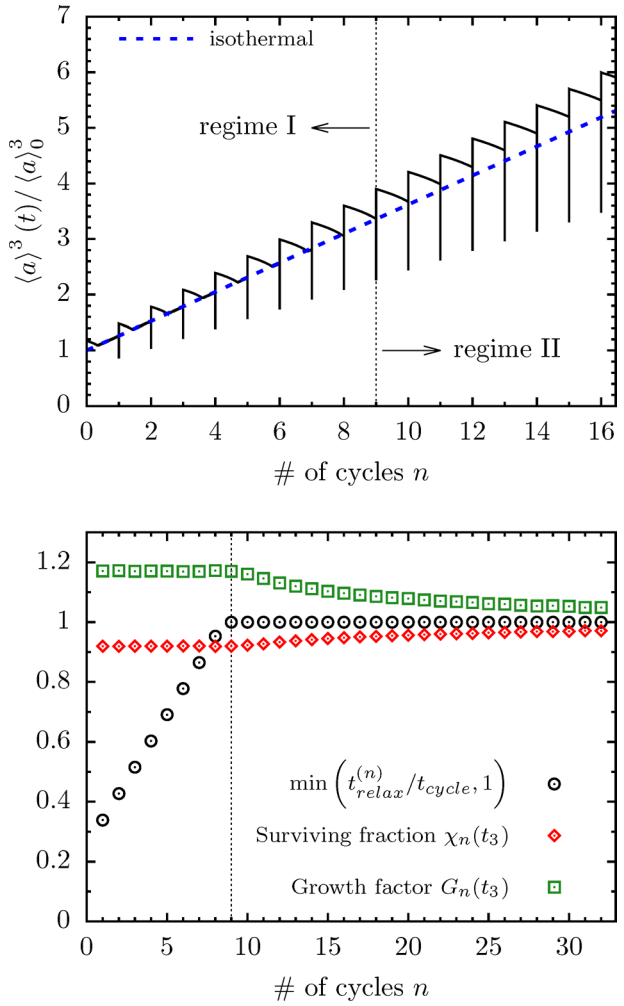

Figure 4. Effect of n successive temperature cycles ($t_2 - t_1 = 0$, $\phi_d = 0.329$, $\phi_V(T_L) = 0.599$, $\tilde{t}_{cycle} = 0.0608$) on the temporal evolution of the average particle radius cubed (top), the relaxation time $t_{relax}^{(n)}$, the fraction of particles that survives dissolution $\chi_n(t_3)$, and the growth factor due to dissolution−regrowth $G_n(t_3)$ (bottom). Results were calculated using the BW growth model. Two growth regimes are observed, the first regime ($t_{relax} < t_{cycle}$) is characterized by slower growth compared to isothermal ripening at T_L (blue dashed line), while the second regime ($t_{relax} > t_{cycle}$) is characterized by faster growth.

for a single cycle, namely, slower growth as compared to isothermal Ostwald ripening (although the differences are very small). If the relaxation time exceeds the cycle time and relaxation becomes incomplete (which for the case analyzed in Figure 4 happens from cycle 9 onward), two effects start to compete: on the one hand, any subsequent cycle will dissolve fewer particles, thus decreasing the growth factor due to dissolution−regrowth $G_n(t_3)$. On the other hand, the decrease in average particle size due to relaxation becomes smaller (as relaxation is incomplete), which increases the impact of the following cycle. As shown in Figure 4, the net effect is an enhanced growth rate as compared to the first regime. More importantly, the growth rate within the second regime is larger than for isothermal ripening, which is the same behavior as is generally observed in experiments.[19−22,24,25]

In Figure 5A, we study the effect of varying the amplitude of a temperature cycle. For visual clarity, only data corresponding to the start of each cycle is shown (as denoted by the symbols). Trends are the same as in Figure 4, but are enhanced as amplitude is increased; i.e., for larger amplitudes the growth rate within the first regime ($t_{relax} < t_{cycle}$) becomes smaller (although the effect is minor) whether in the second regime ($t_{relax} > t_{cycle}$) it becomes larger. For amplitudes larger than some threshold value, the relaxation time of the first cycle already exceeds the cycle time, and only a single regime with faster particle growth as compared to isothermal ripening is observed.

For any of the two growth regimes, we find the net effect of successive cycling is a linear scaling of the average particle radius cubed with time (see Table 1 for correlated coarsening rates), which is the same behavior as for isothermal Ostwald ripening. The linear scaling was found for any case studied and seems general. Experimental measurements (on frozen foods) indicate linear behavior as well;[19,22,29] we herewith show this behavior is caused by the interplay of dissolution−regrowth and relaxation.

The effect of the cycle frequency is analyzed in Figure 5B. Again, two different linear regimes can be observed, depending on the relative magnitude of the cycle time and time needed for relaxation. The cycle number where the first regime enters the second regime increases with increasing cycle time (or decreasing frequency). Interestingly, the coarsening rate appears largely unaffected by changes in cycle frequency.

Finally, the shape of the PSD is analyzed in Figure 6. From the point where relaxation becomes incomplete (cycle 9 for this case), the rescaled PSD at the start of each new cycle slowly evolves to a quasi-stationary shape, which differs from the initial (isothermal) distribution by an absence of the lower tail. In many respects, the evolution toward this quasi-stationary shape is opposite to the evolution of the PSD during relaxation. The quasi-stationary PSD is narrower, stronger peaked, and more symmetric as compared to the initial distribution. For the larger amplitudes studied (results not included for brevity), the quasi-stationary PSD becomes even a little skewed to the left (instead of the right-skewed initial PSD). When this happens, the lower saddle point ($z < \langle z \rangle$), which in Figure 6 is just barely present, completely

DOI: 10.1021/acs.cgd.8b00267
Cryst. Growth Des. 2018, 18, 4952−4962

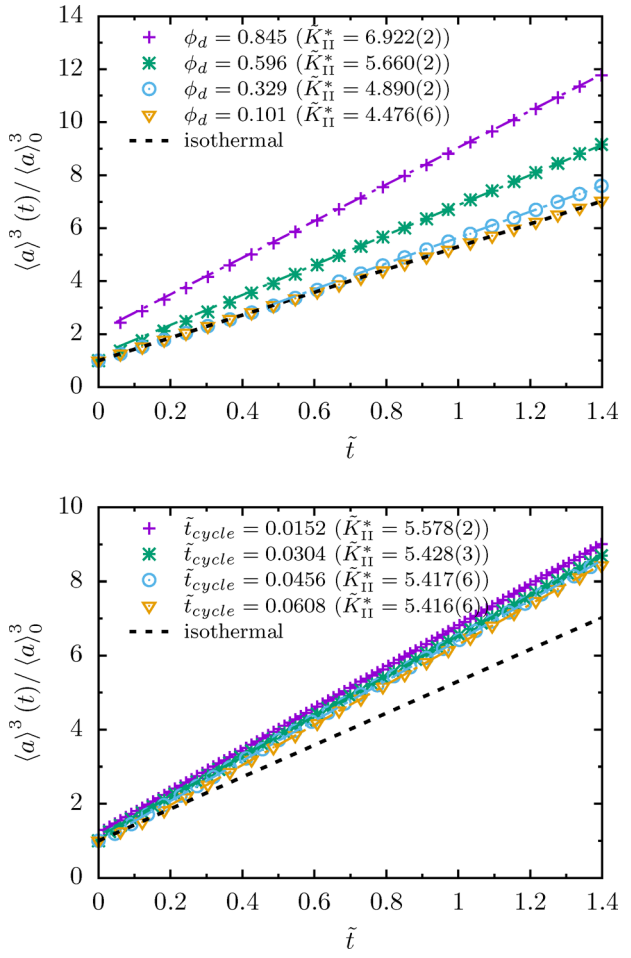

Figure 5. Effect of the cycle amplitude $\phi_d = 1-\phi_V(T_H)/\phi_V(T_L)$ (top) and frequency $1/\tilde{t}_{cycle}$ (bottom) on the temporal evolution of the average particle size cubed at the start of each cycle (symbols). Results are for Case 1 ($t_2 - t_1 = 0$). If not stated otherwise in the legend, $\phi_d = 0.484$, $\phi_V(T_L) = 0.599$, and $\tilde{t}_{cycle} = 0.0608$. Dashed-dotted lines are linear correlations of the data in the second regime; the slope (which corresponds to the coarsening rate $\tilde{K}_{II}^*$) and an estimate of the standard deviation in the last digit are included in the legend. Correlations were developed based on a total of 150 cycles; for visual clarity, only the first few are displayed in this figure. The results in this figure show that for Case 1, the coarsening rate increases with amplitude, but is relatively unaffected by an increase in frequency.

disappears. These results provide a possible explanation for measured crystal-size distributions in igneous rock or magma chambers, which are generally characterized by a slightly left-skewed shape and an absence of the lower saddle point.[23,41]

Although the simple dissolution−regrowth−relaxation model analyzed in this section is able to explain quite some experimental trends, several issues remain open for discussion. First, there is the prediction of two linear regimes, a feature that has so far not been observed experimentally. As the difference in slope of both regimes is rather small, and typical experimental errors are large, it could be this is simply difficult to detect. Second, there is the prediction of slowed-down Ostwald ripening as compared to the isothermal case (first growth regime). On the basis of comparison to available experimental data,[19−22,24,25] this result seems unrealistic and could be an artifact of the simplicity (i.e., $t_2 - t_1 = 0$) of the model. In addition, the insensitivity of the coarsening rate to

Table 1. Effect of Cycle Amplitude ϕ_d and Cycle Time $\tilde{t}_{cycle}$ on the Coarsening Rate $\tilde{K}_I^*$ in Regime I ($\tilde{t}_{relax} < \tilde{t}_{cycle}$) and $\tilde{K}_{II}^*$ in Regime II ($\tilde{t}_{relax} > \tilde{t}_{cycle}$)[a]

		Case 1		Case 2	
ϕ_d	$\tilde{t}_{cycle}$	$\tilde{K}_I^*$	$\tilde{K}_{II}^*$	$\tilde{K}_I^*$	$\tilde{K}_{II}^*$
0.101	0.0608	4.3098(6)	4.476(6)	4.485(1)	4.681(4)
0.329	0.0608	4.270(2)	4.890(2)	5.44(1)	5.966(2)
0.596	0.0608		5.660(2)		9.830(3)
0.845	0.0608		6.922(2)		20.56(2)
0.484	0.0608		5.416(6)		7.971(6)
0.484	0.0456		5.417(6)		8.68(1)
0.484	0.0304		5.428(3)		10.37(1)
0.484	0.0152		5.578(2)		15.30(1)

[a]A comparison between results for Case 1 ($\tilde{t}_2 - \tilde{t}_1 = 0$) and Case 2 ($\tilde{t}_2 - \tilde{t}_1 = 0.0006331$), for $\phi_V(T_L) = 0.599$. Coarsening rates were obtained from a linear correlation to numerically calculated values for $(\langle a \rangle(n\cdot\tilde{t}_{cycle})/\langle a \rangle_0)^3$, with $n \leq 150$ the cycle number (which is an integer). The number in between parentheses is an estimate of the standard deviation in the last digit. All cycle amplitudes and cycle times correspond to those shown graphically in Figures 5 and 9.

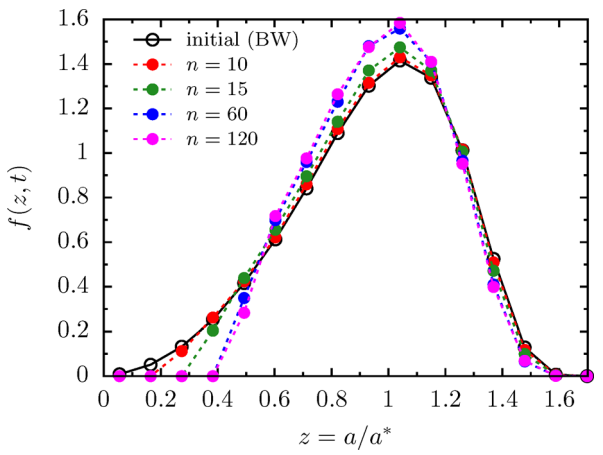

Figure 6. Effect of n successive temperature cycles (for details see Figure 4) on the rescaled PSD. Dotted lines are a guide for the eye. After sufficient cycles, say $n \geq 60$, the PSD approaches a new quasi-stationary form, characterized by the absence of the lower tail and a more symmetric shape.

the cycle frequency is surprising and is difficult to reconcile with experimental results, which generally show an increase of the coarsening rate with increasing frequency.[29] Finally, we note that experimentally measured particle size distributions (e.g., in metallurgy) are usually broader, less-peaked, and more symmetric as compared to the stationary PSD that is obtained from theories for isothermal Ostwald ripening.[3] It is sometimes hypothesized that the discrepancies are due to small, but unavoidable, temperature fluctuations in the experimental setup. Although we find a more symmetric PSD, the model does not correct for the other discrepancies and is therefore unable to confirm this hypothesis.

5.2. Case 2: $t_2 - t_1 > 0$. We now further extend the dissolution−regrowth model by also allowing some Ostwald ripening to take place at the peak temperature T_H of a cycle. In principle we could do a parametric study, where the parameter ψ from eq 25 and the time the system is kept at the peak of the temperature cycle $\tilde{t}_2 - \tilde{t}_1$ are used as additional model parameters. However, it should be clear that any ripening at the elevated temperature will increase the growth factor $G(t_3)$;

DOI: 10.1021/acs.cgd.8b00267
Cryst. Growth Des. 2018, 18, 4952−4962

therefore, there will exist a combination of these parameters that leads to enhanced Ostwald ripening from the first cycle onward and therefore a closer agreement to experimental observations as for Case 1 (absence of first regime). For a fair comparison between the growth models analyzed in this and the previous section, it is thus is more appropriate to consider a realistic system, as a case study.

We choose to calculate ψ for a polycrystalline system of ice in an aqueous solution of sucrose. On the one hand, this is because all relevant material properties for calculating the dimensional prefactor ξ (eq 8) are known for this system (which is quite rare); on the other hand, this choice is made to stay closest to the experiments done on temperature cycling, which for the largest part comprise experiments on frozen sugar solutions and ice cream.[19,22,29,30] For the calculation of material parameters, the reader is referred to the Appendix. It is important to note that the main conclusions and insights of this work are not affected by our choice for this specific system.

To model a typical freeze−thaw cycle, we assume $T_L = -11$ °C, $T_H = -5$ °C, a time at the peak temperature of $t_2 - t_1 = 30$ min, and a time until the next cycle of $t = 48$ h. Further inputs needed are the critical radius at time zero $a^*(t_0)$ [since this defines the time-scale $\tau = a^{*3}(t_0)/\xi(T_L)$ that is needed to relate the real dimensional time at the peak of the temperature fluctuation to dimensionless time], and the mass fraction of sugar before freezing w_0 (as this defines the initial volume-fraction of ice $\phi_V(T_L)$). We use $a^*(t_0) = 30$ μm and $w_0 = 0.28$, which are typical values for stored, frozen foods. This leads to a characteristic time-scale of $\tau = 810$ h (33 days).

The temporal evolution of the PSD, the number of crystals, and the average crystal radius are presented in Figure 7. As the rescaled PSD at time t_1 extends all the way to $z = 0$, the transient ripening at the elevated temperature T_H proceeds from the start by a decreasing number of crystals and an increasing average crystal radius (see inset of Figure 7C). Note the increase is much faster than at the low temperature T_L, a result primarily caused by the strong increase of the binary diffusion coefficient with temperature.[11] Due to the Ostwald ripening at the elevated temperature, the crystal size at time t_2 is larger than for a dissolution−regrowth mechanism only (Section 5.1), leading to an enhanced growth factor $G(t_3)$. As can be observed, the enhancement of the growth factor is sufficient to make up for the decrease of the average crystal radius during subsequent relaxation. For a dissolution−ripening−regrowth mechanism, the net effect of a (realistic) temperature cycle plus complete relaxation is thus enhanced growth as compared to the isothermal case.

Figures 8−9 show the results for successive cycling. As in the previous section, two linear regimes can be observed if, initially, the relaxation time is smaller than the cycle time, whereas only one regime is observed if the relaxation time is larger. For the realistic example chosen, however, the difference in slope between the two regimes can barely be seen with the naked eye. For both regimes, the coarsening rate exceeds that of isothermal Ostwald ripening, which brings the results for Case 2 closer to those obtained from experiments than the results for Case 1. The effect of cycling amplitude and frequency is also much more pronounced than for the growth mechanism analyzed in the previous section. Particularly noteworthy is the strong enhancement of Ostwald ripening as the frequency is increased, which is a second indication that Case 2 is more realistic than Case 1. For numerical comparison

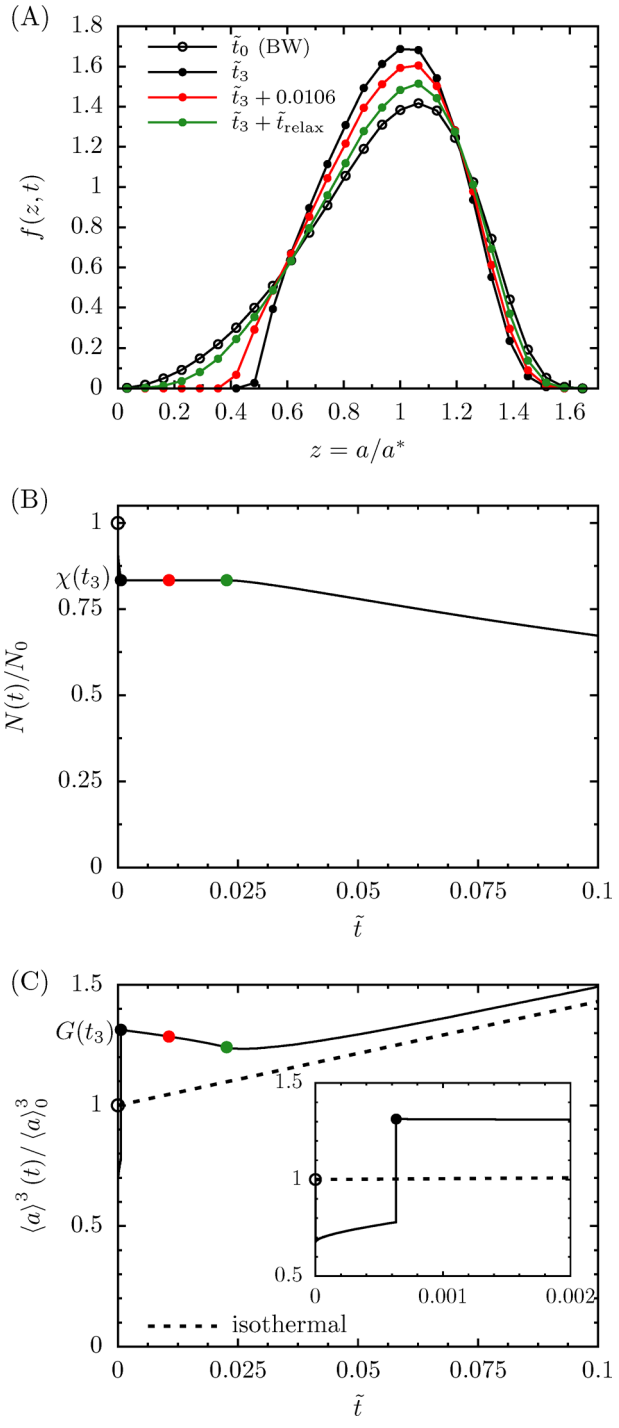

Figure 7. Effect of a typical freeze−thaw cycle ($t_2 - t_1 = 30$ min, $T_L = -11$ °C, $T_H = -5$ °C, $t_{cycle} = 48$ h) on the size distribution (A), the number (B), and the average size (C), of ice crystals dispersed through an aqueous solution of sucrose. The rescaled crystal-size distribution at time t_0 is assumed self-similar, with critical radius $a^*(t_0) = 30$ μm. The initial mass fraction of sucrose, that is before formation of any ice, was set to $w_0 = 0.28$. All results are obtained using the growth rate of the BW theory (eq 9). Both, the stationary form of the BW distribution and the correct coarsening rate are retained after sufficiently long simulation time. In (C), results are compared to those for isothermal Ostwald ripening at temperature T_L (dashed line); the inset shows the effect of the enhanced ripening that takes place at the elevated temperature T_H.

DOI: 10.1021/acs.cgd.8b00267
Cryst. Growth Des. 2018, 18, 4952−4962

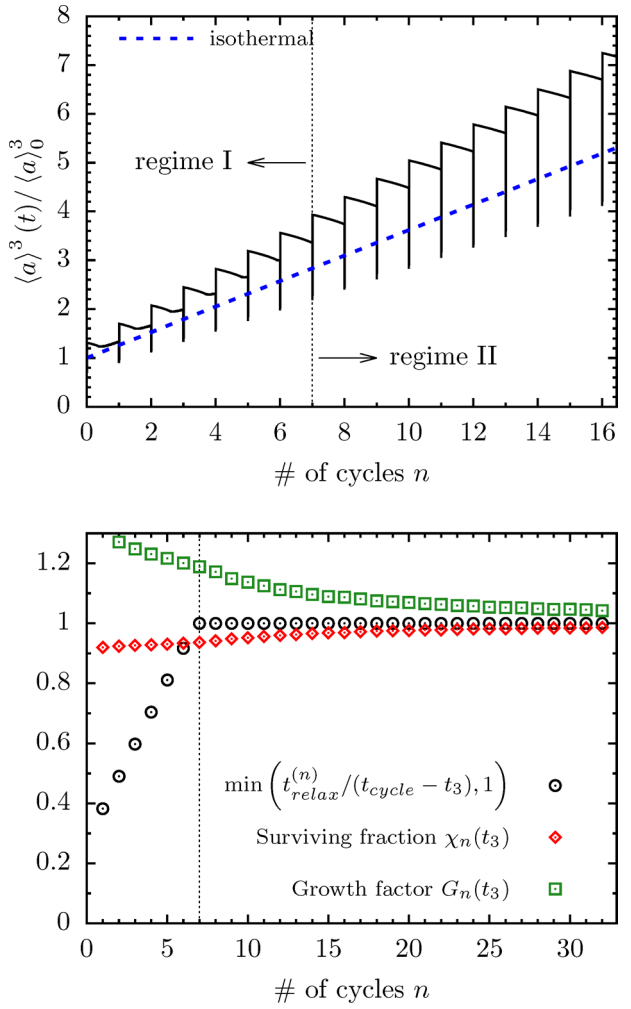

Figure 8. Effect of n successive freeze−thaw cycles in an aqueous solution of sucrose (details as in Figure 7) on the temporal evolution of the average ice crystal radius cubed (top), the relaxation time $t_{relax}^{(n)}$, the fraction of crystals that survives dissolution $\chi_n(t_3)$, and the growth factor due to dissolution-ripening-regrowth $G_n(t_3)$ (bottom). Results were calculated using the BW growth model. In the top figure, the dynamics of isothermal Ostwald ripening at the low temperature T_L are included for comparison (blue dashed line).

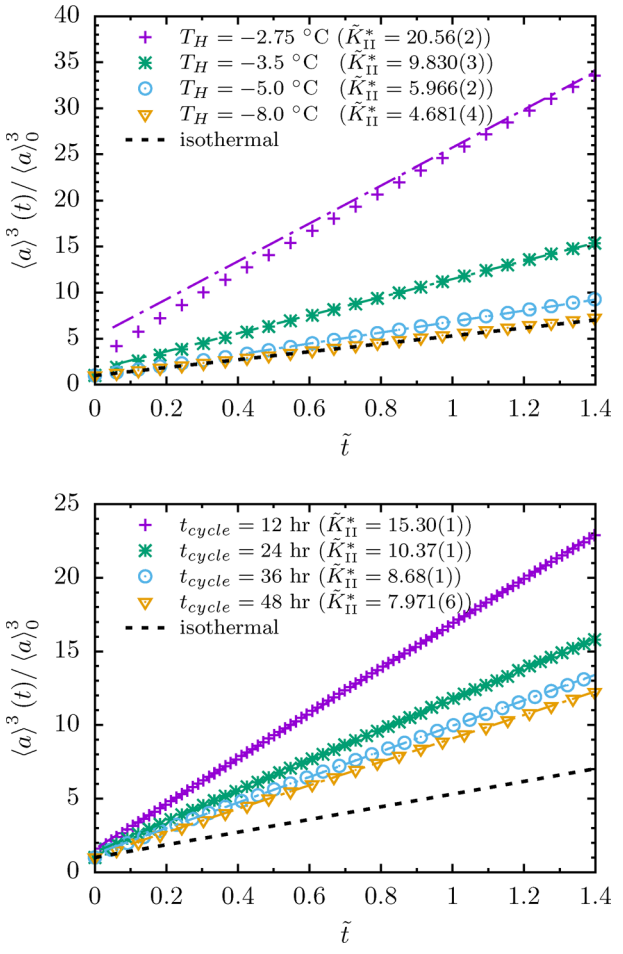

Figure 9. Effect of the amplitude (top) and frequency (bottom) of freeze-thaw cycling in aqueous solutions of sucrose on the temporal evolution of the average crystal radius cubed at the start of each cycle (symbols). If not stated otherwise in the legend, details are as in Figure 7, but with $T_H = -4$ °C. Amplitude and frequency were chosen to match those analyzed for Case 1 in Figure 5, i.e., $T_H = -2.75$ °C ⇔ $\phi_d = 0.845$, $t_{cycle} = 12$ h ⇔ $\tilde{t}_{cycle} = 0.0152$, and so on. Dashed-dotted lines are linear correlations of the data in the second regime; the slope (which corresponds to the coarsening rate $\tilde{K}_{II}^*$) and an estimate of the standard deviation in the last digit are included in the legend. Correlations were developed based on 150 cycles; for visual clarity only the first few are displayed in this figure. The results in this figure show that for Case 2, the coarsening rate is much more strongly affected by changes in amplitude or frequency as compared to Case 1.

of the values for the coarsening rates obtained in this and the previous section, see Table 1.

The evolution of the PSD with the number of cycles applied is similar to that analyzed in the previous section, for Case 1. For brevity, results are not included.

5.3. Validity of Assumptions. There are various assumptions underlying the model of Section 4 that require some further discussion.

First, there is the preserved spherical shape of the particles during cooling, which neglects the possibility of anisotropic particle growth due to either morphological instability[37−39] or the roughening transition[42,43] (specifically if the roughening transition temperature differs between different crystal faces). If for any reason particles would grow anisotropically, we speculate these particles to dissolve more easily during subsequent heating. The net effect would be a larger growth factor per cycle as compared to the case where all particles remain spherical, leading to a stronger enhancement of Ostwald ripening due to temperature cycling.

The roughening transition could have a further effect. If during cooling the particle surface smoothens (which could happen if the temperature falls below the roughening transition temperature and supersaturation is small enough to prevent kinetic roughening[44]), particle growth could become limited by attachment kinetics instead of mass transfer through the bulk matrix. The quadratic scaling ($da^2 \propto dt$) for regrowth (eq 20) would then lose its validity and become linear ($da \propto dt$) instead.[3] The net effect of this asymmetric scaling for dissolution and regrowth would be that particles continue to dissolve with each new cycle, irrespective of whether any relaxation has taken place in between cycles. It is likely this would destroy the linear scaling of the average particle radius cubed with time, which suggests that kinetically limited growth is not very relevant here.

DOI: 10.1021/acs.cgd.8b00267
Cryst. Growth Des. 2018, 18, 4952−4962

Finally, there is the assumption of instant thermal equilibration. Clearly, this is an oversimplification, expected to be reasonable only for the surface of a product. If thermal equilibration is incomplete, the local amplitude would be smaller than based on the external temperature. Moreover, gradients in temperature could develop, which can alter the coarsening process.[45] Having that said, we should note that even if only the surface of a product is affected by thermal cycling, this could have a negative impact on product quality. For products where this is the issue (e.g., frozen foods), the model developed seems reasonable.

6. SUMMARY AND CONCLUSIONS

We developed a simulation method for describing the effect of thermal cycling on Ostwald ripening of spherical particles in a binary solution. The model assumes growth and dissolution are limited by mass-transfer through the bulk solution, both for isothermal conditions, and during heating or cooling. The effect of a temperature cycle was modeled by the following sequence of events:

(1) Dissolution on heating
(2) Ripening by (transient) Ostwald ripening at elevated temperature
(3) Regrowth on remaining particles on cooling
(4) Relaxation by (transient) Ostwald ripening at lower temperature

Complete dissolution of the smaller particles during heating (event 1), followed by regrowth on the remaining particles during cooling (event 3), increases the average particle size. Ripening at the elevated temperature (event 2) enhances this effect. The relaxation that takes place after cooling back to the initial temperature (event 4) primarily involves growing back the lower tail of the particle-size distribution (involving the dissolved fines). Relaxation is therefore essential for a subsequent cycle to decrease the amount of particles and thereby to increase the average particle size. During the largest part of the relaxation, the average particle size decreases, which partially offsets the increase in average particle size induced by dissolution−ripening−regrowth (events 1−3).

We find that the interplay of all four processes is required to capture experimental trends: the relaxation of the particle-size distribution in between temperature spikes (event 4) is ultimately responsible for a linear scaling of the cubed average crystal radius with time, in line with generally observed behavior in temperature cycling experiments on (partially) frozen foods and binary solutions. We further find that the observed increase of the coarsening rate (which depends on the temperature cycling amplitude and frequency) relative to isothermal coarsening, can be reproduced convincingly only if transient coarsening takes place at the higher temperature of each cycle (event 2). We thus suggest a new mechanism to explain how and why temperature cycling increases the coarsening rate of Ostwald ripening. This mechanism is characterized by a 4-fold dissolution−ripening−regrowth−relaxation process.

The developed simulation method could prove valuable for predicting the stability (and thus the quality) of dispersed-phase materials such as frozen foods: given (an estimate of) the evolution of the temperature profile within the product, our method could be used to estimate the evolution of the number of crystals, the crystal-size distribution, and the average crystal size.

APPENDIX: MATERIAL PROPERTIES

We here list all the material parameters and model inputs needed for describing isothermal Ostwald ripening of ice dispersed in an aqueous solution of sucrose. For more details, the reader is referred to a previous work.[11]

The equilibrium volume-fraction of ice ϕ_V is related to the initial mass fraction of sucrose in the system w_0 (where initial means before formation of any ice) and temperature T through the mass-fraction $\phi_m = 1 - w_0/w_{s,eq}(T)$, according to

$$\phi_V(w_0, T) = \frac{\phi_m \nu^\beta}{\phi_m \nu^\beta + (1 - \phi_m)\nu^\alpha} \tag{29}$$

The equilibrium mass fraction of sucrose in the matrix is obtained from the following correlation of experimental freezing-point depression data

$$w_{s,eq}(T) = \frac{T}{a_0 T - a_1} \tag{30}$$

with $a_0 = 1.195$ and $a_1 = 5.781$, and $T > -14$°C.

The material properties defining the dimensional pre-factor ξ of the growth rate (eq 7) were calculated based on various correlations to experimental data, as listed in our previous work. We here only present a correlation based on these experimental fits, as

$$^{10}\log \xi(T) = a_0 + a_1 T + a_2 T^2 + a_3 T^3 + a_4 T^4 \tag{31}$$

with ξ in units μm^3/min, $a_0 = 2.8425$, $a_1 = 0.50262$, $a_2 = 0.034348$, $a_3 = 0.0016574$, $a_4 = 3.3152 \times 10^{-5}$, and $-14 < T < -1.5$°C. This correlation is accurate to within a few percent.

As shown in our previous work, use of eqs 29−31 allows a very reasonable prediction of isothermal coarsening rates of ice, with deviations to experiments by less than a factor 2.

AUTHOR INFORMATION

Corresponding Authors

*(T.v.W.) E-mail: thijs.van-westen@itt.uni-stuttgart.de.
*(R.D.G.) E-mail: Rob.Groot@unilever.nl.

ORCID

Thijs van Westen: 0000-0002-0878-8731

Notes

The authors declare no competing financial interest.

ACKNOWLEDGMENTS

This work is part of the Industrial Partnership Programme "Hybrid Soft Materials" that is carried out under an agreement between Unilever Research and Development B. V. and The Netherlands Organisation for Scientific Research (NWO). The work was performed at Unilever Vlaardingen and the NWO research institute AMOLF. We thank Prof. Bela Mulder for a critical reading of the manuscript.

REFERENCES

(1) Ostwald, W. Über die vermeintliche Isomerie des roten und gelben Queck-silberoxyds und die Oberlfächenspannung fester Körper. *Z. Phys. Chem.* **1900**, *34*, 495−503.
(2) Ostwald, W. *Analytisch Chemie*, 3rd ed.; Engelmann: Leipzig, 1901; p 23.
(3) Ratke, L.; Voorhees, P. W. *Growth and Coarsening*, 1st ed; Springer: Berlin, 2002.
(4) Lifshitz, I. M.; Slyozov, V. V. The kinetics of precipitation from supersaturated solid solutions. *J. Phys. Chem. Solids* **1961**, *19*, 35−50.

DOI: 10.1021/acs.cgd.8b00267
Cryst. Growth Des. 2018, 18, 4952−4962

(5) Wagner, C. Theorie der Alterung von Niederschlägen durch Umlösen (Ostwald-Reifung). *Z. Elektrochem.* **1961**, *65*, 581−591.
(6) Mullins, W. W. The statistical self-similarity hypothesis in grain growth and particle coarsening. *J. Appl. Phys.* **1986**, *59*, 1341.
(7) Wang, K. G.; Glicksman, M. E.; Rajan, K. Modeling and simulation for phase coarsening: A comparison with experiment. *Phys. Rev. E* **2004**, *69*, 061507.
(8) Ardell, A. J.; Ma, Y. Coarsening of Ni-Ge solid-solution precipitates in 'inverse' Ni_3Ge alloys. *Mater. Sci. Eng., A* **2012**, *550*, 66−75.
(9) Pletcher, B. A.; Wang, K. G.; Glicksman, M. E. Experimental, computational and theoretical studies of δ' phase coarsening in Al-Li alloys. *Acta Mater.* **2012**, *60*, 5803−5817.
(10) Thompson, J. D.; Gulsoy, E. B.; Voorhees, P. W. Self-similar coarsening: A test of theory. *Acta Mater.* **2015**, *100*, 282−289.
(11) van Westen, T.; Groot, R. D. Predicting recrystallization kinetics of ice in aqueous sugar solutions. *Cryst. Growth Des.* **2018**, *18*, 2405−2416.
(12) Ardell, A. J. The effect of volume fraction on particle coarsening: Theoretical considerations. *Acta Metall.* **1972**, *20*, 61−71.
(13) Brailsford, A. D.; Wynblatt, P. The dependence of Ostwald ripening kinetics on particle volume fraction. *Acta Metall.* **1979**, *27*, 489−497.
(14) Tokuyama, M.; Kawazaki, K. Statistical-mechanical theory of coarsening of spherical droplets. *Phys. A* **1984**, *123*, 386−411.
(15) Marqusee, J. A.; Ross, J. Theory of Ostwald ripening: Competitive growth and its dependence on volume fraction. *J. Chem. Phys.* **1984**, *80*, 536−543.
(16) Enomoto, Y.; Tokuyama, M.; Kawasaki, K. Finite volume fraction effects on Ostwald ripening. *Acta Metall.* **1986**, *34*, 2119−2128.
(17) Marsh, S. P.; Glicksman, M. E. Kinetics of phase coarsening in dense systems. *Acta Mater.* **1996**, *44*, 3761−3771.
(18) Glicksman, M. E.; Wang, K. G.; Marsh, S. P. Diffusional interactions among crystallites. *J. Cryst. Growth* **2001**, *230*, 318−327.
(19) Donhowe, D. P.; Hartel, R. W. Recrystallization of ice during bulk storage of ice cream. *Int. Dairy J.* **1996**, *6*, 1209−1221.
(20) Boonsumrej, S.; Chaiwanichsiri, S.; Tantratian, S.; Suzuki, T.; Takai, R. Effects of freezing and thawing on the quality changes of tiger shrimp (Penaeus monodon) frozen by air-blast and cryogenic freezing. *J. Food Eng.* **2007**, *80*, 292−299.
(21) Ullah, J.; Takhar, P. W.; Sablani, S. Effect of temperature fluctuations on ice-crystal growth in frozen potatoes during storage. *LWT-Food Sci. Technol.* **2014**, *59*, 1186−1190.
(22) Ndoye, F. T.; Alvarez, G. Characterization of ice recrystallization in ice cream during storage using the focused beam reflectance measurement. *J. Food Eng.* **2015**, *148*, 24−34.
(23) Simakin, A. G.; Bindeman, I. N. Evolution of crystal sizes in the series of dissolution and precipitation events in open magma systems. *J. Volcanol. Geotherm. Res.* **2008**, *177*, 997−1010.
(24) Mills, R. D.; Ratner, J. J.; Glazner, A. F. Experimental evidence for crystal coarsening and fabric development during temperature cycling. *Geology* **2011**, *39*, 1139−1142.
(25) Mills, R. D.; Glazner, A. F. Experimental study on the effects of temperature cycling on coarsening of plagioclase and olivine in an alkali basalt. *Contrib. Mineral. Petrol.* **2013**, *166*, 97−111.
(26) Fennema, O.; Powrie, W. D. Fundamentals of low-temperature food preservation. *Adv. Food Res.* **1964**, *13*, 219−347.
(27) Hartel, R. W. In *The Properties of Water in Foods: ISOPOW 6*; Reid, D. S., Ed.; Blackie Academic Professional: London, 1998; Chapter 10, pp 287−319.
(28) Roos, Y. H. *Phase Transitions in Foods*, 2nd ed; Academic Press: Oxford, 2016.
(29) Flores, A. A.; Goff, H. D. Recrystallization in ice cream after constant and cycling temperature storage conditions as affected by stabilizers. *J. Dairy Sci.* **1999**, *82*, 1408−1415.
(30) Regand, A.; Goff, H. D. Structure and ice recrystallization in frozen stabilized ice cream model systems. *Food Hydrocolloids* **2003**, *17*, 95−102.
(31) Syamaladevi, R. M.; Manahiloh, K. N.; Muhunthan, B.; Sablani, S. S. Understanding the Influence of State/Phase Transitions on Ice Recrystallization in Atlantic Salmon (Salmo salar) During Frozen Storage. *Food Biophysics* **2012**, *7*, 57−71.
(32) Voorhees, P. W. The theory of Ostwald ripening. *J. Stat. Phys.* **1985**, *38*, 231−252.
(33) Bird, R. B.; Stewart, W. E.; Lightfoot, E. N. *Transport Phenomena*, 2nd ed; John Wiley & Sons: New York, 2002.
(34) Taylor, R.; Krishna, R. *Multicomponent Mass Transfer*, 1st ed; John Wiley & Sons: New York, 1993.
(35) Zener, C. Theory and growth of spherical precipitates from solid solution. *J. Appl. Phys.* **1949**, *20*, 950.
(36) Aaron, H. B.; Fainstein, D.; Kotler, G. R. DiffusionLimited Phase Transformations: A Comparison and Critical Evaluation of the Mathematical Approximations. *J. Appl. Phys.* **1970**, *41*, 4404.
(37) Mullins, W. W.; Sekerka, R. F. Morphological stability of a particle growing by diffusion or heat flow. *J. Appl. Phys.* **1963**, *34*, 323−229.
(38) Mullins, W. W.; Sekerka, R. F. Stability of a planar interface during solidification of a dilute binary alloy. *J. Appl. Phys.* **1964**, *35*, 444−451.
(39) Langer, J. S. Instabilities and pattern formation in crystal growth. *Rev. Mod. Phys.* **1980**, *52*, 1−30.
(40) Marqusee, J. A.; Ross, J. Kinetics of phase transitions: Theory of Ostwald ripening. *J. Chem. Phys.* **1983**, *79*, 373−378.
(41) Bindeman, I. N. Crystal sizes in evolving silicic magma chambers. *Geology* **2003**, *31*, 367−370.
(42) Weeks, J. D. In *Ordering in Strongly Fluctuating Condensed Matter Systems. NATO Advanced Study Institute Series (Series B: Physics)*, Vol. *50*; Riste, T., Ed.; Springer: Boston, MA, 1980; p 293.
(43) Bennema, P. Morphology of crystals determined by α factors, roughening temperature, F faces and connected nets. *J. Phys. D: Appl. Phys.* **1993**, *26*, B1−B6.
(44) Bennema, P.; van der Eerden, J. P. In *The Morphology of Crystals*; Sunagawa, I., Ed.; Terra: Tokyo, 1987; pp 1−75.
(45) Snyder, V. A.; Akaiwa, N.; Alkemper, J.; Voorhees, P. W. The influence of temperature gradients on Ostwald ripening. *Metall. Mater. Trans. A* **1999**, *30*, 2341−2348.

DOI: 10.1021/acs.cgd.8b00267
Cryst. Growth Des. 2018, 18, 4952−4962